Staging of cognitive deficits and neuropathological and ultrastructural changes in streptozotocin-induced rat model of Alzheimer's disease

Knezović, Ana; Osmanović-Barilar, Jelena; Ćurlin, Marija; Hof, Patrick R.; Šimić, Goran; Riederer, Peter; Šalković-Petrišić, Melita

Source / Izvornik: **Journal of Neural Transmission, 2015, 122, 577 - 592**

Journal article, Accepted version
Rad u časopisu, Završna verzija rukopisa prihvaćena za objavljivanje (postprint)

https://doi.org/10.1007/s00702-015-1394-4

Permanent link / Trajna poveznica: https://urn.nsk.hr/urn:nbn:hr:105:301217

Special issue in honour of Professor Siegfried Hoyer

Staging of cognitive deficits and neuropathological and ultrastructural changes in streptozotocin-induced rat model of Alzheimer's disease

Ana Knezovic[1], Jelena Osmanovic-Barilar[1], Marija Curlin[2], Patrick R. Hof[3], Goran Simic[4], Peter Riederer[5], Melita Salkovic-Petrisic[1]

[1]Department of Pharmacology and Croatian Institute for Brain Research, University of Zagreb School of Medicine, Salata 11, 10000 Zagreb, Croatia
[2]Department of Histology and Croatian Institute for Brain Research, University of Zagreb School of Medicine, Salata 12, 10000 Zagreb, Croatia
[3]Fishberg Department of Neuroscience and Friedman Brain Institute, Icahn School of Medicine at Mount Sinai, New York, NY 10029, USA
[4]Department of Neuroscience, Croatian Institute for Brain Research, University of Zagreb School of Medicine, Salata 12, 10000 Zagreb, Croatia
[5]Center of Psychic Health, Clinic and Policlinic for Psychiatry and Psychotherapy, University Hospital Würzburg, D-97080 Würzburg, Germany

*Corresponding author: Melita Salkovic-Petrisic
e-mail address: melitas@mef.hr
phone number: +38514590219
postal address: Department of Pharmacology
University of Zagreb School of Medicine
Salata 11
10 000 Zagreb
Croatia

Abstract

Sporadic Alzheimer's disease (sAD) is the most common form of dementia. Rats injected intracerebroventricularly with streptozotocin (STZ-icv) develop insulin-resistant brain state and represent a non-transgenic sAD model with a number of AD-like cognitive and neurochemical features. We explored cognitive, structural and ultrastructural changes in the brain of the STZ-icv rat model over a course of nine months.

Cognitive functions were measured in the STZ-icv- (0.3, 1 and 3 mg/kg) and age-matched control rats by Passive avoidance test. Structural changes were assessed by Nissl and Bielschowsky silver staining. Immunohistochemistry and electron microscopy analysis were used to detect amyloid β- ($A\beta_{1-42}$) and hyperphosphorylated tau (AT8) accumulation and ultrastructural changes in the brain.

Memory decline was time- (≤3 months/acute, ≥3 months/progressive) and STZ-icv dose-dependent. Morphological changes were manifested as thinning of parietal cortex (≥1 month) and corpus callosum (9 months), and were more pronounced in the 3 mg/kg STZ group. Early neurofibrillary changes (AT8) were detected from 1 month onward in the neocortex, and progressed after 3 months to the hippocampus. Intracellular $A\beta_{1-42}$ accumulation was found in the neocortex at 3 months following STZ-icv treatment, while diffuse $A\beta_{1-42}$-positive plaque-like formations were found after 6 months in the neocortex and hippocampus. Ultrastructural changes revealed enlargement of Golgi apparatus, pyknotic nuclei, and time-dependent increase in lysosome size, number, and density.

Our data provide a staging of cognitive, structural/ultrastructural, and neuropathological markers in the STZ-icv rat model that in many aspects seems to be generally comparable to stages seen in human sAD.

Keywords: Alzheimer's disease, streptozotocin, amyloid protein, tau protein, lysosomes, cognitive decline

Introduction

Alzheimer's disease (AD) is the most common form of dementia, clinically characterized by a progressive memory loss. The major neuropathological hallmarks of AD are senile (amyloid) plaques and neurofibrillary tangles (NFTs) that demonstrate regionally specific distribution in cerebral cortex and in certain subcortical nuclei (Braak and Braak 1991, 1995; Selkoe 2001; Thal et al. 2002b). Amyloid $\beta_{1\text{-}42}$ ($A\beta_{1\text{-}42}$) is the main component of senile plaques, which may occur as diffuse plaques, intermingled amongst neuronal processes that appear to remain unaffected by this process, and compact or cored plaques that damage brain tissue. The latter induce microglia and astrocyte activation, and are typically surrounded by dystrophic, tau-containing neurites. Hyperphosporylated tau protein is the main component of NFTs, which are located in the cytoplasm of neuronal cell bodies and neuritic processes (Buee et al. 2000; Hinrichs et al. 2012; Simic et al. 1998).

Contrary to the rare and inherited early-onset form of AD, the cause of the prevailing, sporadic late-onset AD form (sAD) is unknown. In addition to the various mechanisms of neural degeneration, like mitochondrial dysfunction (Diana et al. 2008) and oxidative stress (Leuner et al. 2012; Simic et al. 2009; Thome et al. 1997; Völkel et al. 2006), or environmental factors (Shaw and Höglinger 2008) suggested to play a role in the etiopathogenesis of sAD, evidence supports the concept of brain insulin resistance and metabolic dysfunction being important mediators of pathophysiological changes in sAD (Correia et al. 2011; De Felice et al. 2014; de la Monte and Tong 2014; Hoyer 2004; Salkovic-Petrisic et al. 2009). Modelling of brain insulin resistance is therefore relevant in this respect but has not been sufficiently studied. The identification of disease-causing mutations in proteins such as Aβ precursor protein (APP) and presenilins 1 and 2 (PS1, PS2) as well as pathogenic mutations in tau protein, resulted in development of many transgenic mice AD models (Lithner et al. 2011). However, such models are representative for rare familial AD forms and their reliability as models for sAD has been recently questioned as well as their actual use in AD drug discovery (Bales 2012; Zach and Ashe 2010). Amyloid-related gene manipulation in transgenic mice AD models is inevitable starting point as antecendent to Aβ pathology as well as to brain insulin dysfunction whose development differs between the transgenic mice AD models (Chen et al. 2013; Niwa et al. 2002; Pedersen et al. 2006; Pedrós et al. 2014). For this reason trangenic mice AD models are inappropriate for exploring the cause, onset and development of the pathological Aβ deposition in the brain in a condition that is not associated with mutations of the *APP/PS1* genes and in which brain insulin dysfunction might precede Aβ pathology (like in sAD).

A different approach that does not involve genetic engineering has been used to generate a non-transgenic rat model of insulin resistance in the brain by intracerebroventricular (icv) injection of streptozotocin (STZ-icv model) (Lanner and Hoyer 1998). STZ (2-deoxy-2-(3-(methyl-3-nitrosoureido)-D-glucopyranose)) is a cytotoxic compound that acts selectively on insulin producing/secreting cells and causes type 1 diabetes mellitus in adult rats following parenteral administration at high doses (Szkudelski 2001). Multiple parenteral treatments with low-to-moderate STZ doses cause insulin resistance and type 2 diabetes mellitus by affecting insulin receptor (IR) signalling (Blondel and Portha 1989; Giorgino et al. 1992; Kadowaki et al. 1984). Icv administration of low STZ doses does not induce a systemic diabetic condition in rats, but has been convincingly shown to induce insulin-resistant brain state characterized by altered tyrosine kinase activity of IR and dysfunctional signalling downstream the IR signaling pathways (Agrawal et al. 2010, 2011; Grünblatt et al. 2007; Lester-Coll et al. 2006; Osmanovic-Barilar et al. 2014; Salkovic-Petrisic et al. 2006; Steen et al. 2005), accompanied by a decrease in brain glucose and energy metabolism (Hoyer and Lannert 2007; Lannert and Hoyer 1998; Nitsch and Hoyer 1991; Plaschke and Hoyer 1993). Additionally, the STZ-icv rat model has been demonstrated to develop remarkable behavioral

and neuropathological AD-like features, in particular cognitive (Mayer et al. 1990) and brain cholinergic deficits (Hellweg et al. 1992), as well as oxidative stress (Correia et al. 2013; Sharma and Gupta 2001), neuroinflammation, and astrogliosis (Chen et al. 2013; Javed et al. 2011; Kraska et al. 2012; Prickaerts et al. 1999, 2000; Rodrigues et al. 2010; Shoham et al. 2003, 2007). Severely affected STZ-icv rats also demonstrate extensive cell loss, inferred from increase in the volume of the ventricular system (Kraska et al. 2012; Prickaerts et al. 2000; Shoham et al. 2003), and a significant enlargement of the trans-Golgi compartment in cortical neurons at the ultrastructural level (Grieb et al. 2004). In addition, increased $A\beta_{1-42}$ and hyperphosphorylated tau immunoreactivity have been detected in the hippocampus of STZ-icv rats and mice (Chen et al. 2013; Correia et al. 2013; Deng et al. 2009; Kosaraju et al. 2013; Shingo et al. 2012). Accumulation of Aβ in the cerebral microvasculature (cerebral amyloid angiopathy, CAA) has been observed first in the meningeal capillaries (Salkovic-Petrisic et al. 2006), progressing subsequently to the intracortical blood vessels of STZ-icv rats (Salkovic-Petrisic et al. 2011).

With the exception of a long-term follow-up of CAA development (Salkovic-Petrisic et al. 2013) and dysfunction in IR signaling cascade (Osmanovic-Barilar et al. 2014), there have been no reports on neurochemical or neuropathological changes in the brain or of cognitive deficits in STZ-icv models investigated in periods of more than 6 months after STZ injection. To characterize and validate the model better, in this 9-month follow-up study, we have assessed the onset, development, and progression of $A\beta_{1-42}$ and hyperphosphorylated tau immunopositive lesions, ultrastructural changes in the brain, as well as cognitive deficits in the STZ-icv rats as a function of STZ dose and post-treatment time.

Materials and Methods

Chemicals

Streptozotocin was purchased from Sigma-Aldrich Chemie (Munich, Germany). Phospho-PHF-tau pSer202/Thr205 monoclonal antibody (AT8, cat. no. MN1020) was purchased from Thermo Scientific (Waltham, MA, USA). Monoclonal antibodies against amyloid β_{1-42} were purchased from Signet, (Signet Laboratories, Inc., Dedham, MA, USA, 2006, cat. No. 39142) and from Covance (Princeton, NJ, USA; clone 12F4, cat. No. 39142 and cat. No. 39136). Vectastain Elite ABC Kit (Cat. No. PK-6200) while normal goat serum (S-1000), biotinylated goat anti-mouse IgG antibody (cat. no. BA-9200) and ImmPACT AEC peroxidase substrate (cat. no. SK-4205) were purchased from Vector Laboratories (Burlingame, CA, USA). Paraformaldehyde was purchased from Sigma Aldrich (cat. no. 16005, St. Louis, MO, USA). MultiLink–HRP kit was purchased from Biogenex (cat. no. LP000-UL, San Ramon, CA, USA) and Romulin AEC chromogen was purchased from Biocarta (cat. no. RAEC810L, San Diego, CA, USA).

Animals

Three-month-old male Wistar rats weighing 280-350 g (Department of Pharmacology, University of Zagreb School of Medicine) were used in all experiments. The rats were kept 2-3 per cage in a room with a 12 h light/12 h dark cycle (lights on 07:00 – 19:00 h), and the room temperature and humidity set in the range of 21-25°C and 40-70% respectively. All animals were kept on standardized food pellets and water *ad libitum*.

Surgery

Rats were subjected to deep general anesthesia (chloral hydrate 300 mg/kg, ip, Merck, Darmstadt, Germany), followed by icv injection of STZ (0.3, 1 or 3 mg/kg, dissolved in 0.05 M citrate buffer, pH 4.5, bilaterally 2 μl/ventricle split in two doses given on day 1 and 3), according to the procedure first described by Noble et al. (1967) and used elsewhere (Grünblatt et al. 2007; Lackovic and Salkovic 1990; Osmanovic-Barilar et al. 2014; Salkovic-Petrisic et al. 2011; Salkovic et al. 1995). Control animals were given an equal volume of vehicle icv by the same procedure on day 1 and 3.

Experimental design

STZ-icv (0.3, 1, or 3 mg/kg) and respective age-matched control (treated icv with 0.05 M citrate buffer, pH 4.5) animals were sacrificed in after 1 week, and 1, 3, 6, or 9 months following the treatment, respectively. Cognitive testing was performed immediately before sacrifice at each time-point (N = 8-10 per group, four groups per experiment: control, STZ 0.3 mg/kg, STZ 1 mg/kg, STZ 3 mg/kg). In additional set of experiments rats treated with high (3 mg/kg) STZ-icv dose and age-matched controls were sacrificed 2 weeks, and 1, 3, 6 and 9 months after the treatment (two groups per experiment: control, STZ 3 mg/kg). Animals were euthanised in deep anaesthesia (thiopental:diazepam 50 mg/kg:6 mg/kg intraperitoneally) followed by decapitation in all experiments.

Cognitive testing

Memory functions were tested by passive avoidance test with a step-through type passive avoidance task (Ugo Basile, Comerio, Italy) utilizing the natural preference of rats for dark environments. It is a fear-motivated avoidance task in which rats learn to refrain from stepping through a door to an apparently safer but previously punishment-related dark compartment. The latency to refrain from crossing into the punishing compartment serves as an index of the ability to avoid, and allows memory assessment. Those rats that had no alterations in memory functions (vehicle-treated controls) had to remember that a foot shock would follow entering the dark compartment (therefore had to stay longer in the lit compartment on the test day). In case of impaired memory functions, rats would not

associate the foot shock with the dark environment and spend less time in the lit compartment. Passive avoidance test performance lasts for three days starting with a habituation day to make the rat familiar with the environment (without foot shock, or pre-shock latency), followed by a training day in which foot shock (0.3-0.5 mA, depending on the rat weight, duration 2 s) is delivered; and finally a testing day (without foot shock). Time required for entrance of a rat in the dark compartment was measured with a cut-off time of 5 min. In all of the experiments, passive avoidance test was performed only once per group/experiment.

Tissue preparation

Animals were deeply anesthetized with chloral hydrate (300 mg/kg ip) or thiopental:diazepam (50 mg/kg:6 mg/kg ip) and perfused with saline followed by 4% paraformaldehyde, pH 7.4 in a standard procedure. Brains were quickly removed and embedded in paraffin, then cut on a sliding microtome into 8 μm-thick sections. Tissue sections were mounted on slides and dried by leaving the slide at room temperature overnight. Tissue sections for Aβ immunohistochemistry were obtained from animals in experiments (3 mg STZ-icv only) different from those used for cognitive testing and structural tau protein and electron microscopy analysis.

Immunohistochemistry

The slides were first deparaffinized and rehydrated. Before immunohistochemical staining with AT8 and monoclonal antibodies against $A\beta_{1-42}$, slides were subjected to antigen retrieval step (1 h in 80% formic acid for $A\beta_{1-42}$ immunostaining, and 30 min on 95°C in sodium citrate buffer, pH 6.0) and then washed and incubated in 0.7% H_2O_2 for 15 min. Slides were then washed in TBS (pH 7.6) and blocked with 10% normal goat serum for 1 h and incubated with primary antibodies AT8 (1:100) and $A\beta_{1-42}$ (1:2,000) diluted in TBS with 1% BSA overnight at 4°C. Next day slides (incubated with AT8) were washed and incubated with biotinylated secondary goat anti-mouse antibody for 1 h, followed by incubation with Vectastain ABC kit for 30 min. Immunoreaction was developed by incubation with ABC peroxidase substrate kit for 4 min. Slides were counterstained with haematoxylin for 1 min, washed with H_2O and mounted. Slides incubated with $A\beta_{1-42}$ were incubated with MultiLink kit following the manufacturer's protocol. The reaction was developed by incubation with Romulin AEC chromogen for 4 min. Slides were then counterstained with haematoxylin, washed, dehydrated, and mounted. Specific positive $A\beta_{1-42}$ signal in the rat brain was obtained by antibody purchased from Signet (Dedham, MA, USA). Immunohistochemistry was performed on four sections per brain (number of animals per group: 1-2 for $A\beta_{1-42}$ and 3-4 for AT8). Human AD brain tissue samples were used as a positive control in both AT8 and $A\beta_{1-42}$ immunohistochemistry.

Bielschowsky silver staining

Slides were deparaffinized and rehydrated, and then incubated for 20 min in the dark with a 20% $AgNO_3$ solution. Slides were then washed with dH_2O and incubated for another 15 min with the same solution but with added ammonium, and washed in dH_2O with ammonium. Then slides were incubated for 3-5 min or until they darken in the $AgNO_3$/ammonium solution with developer (20 ml of formalin, a drop of concentrated HNO_3, 0.5 g of citric acid, and 100 ml of dH_2O) and then washed and fixated in 5% sodium thiosulfate for 5 min (Uchihara 2007). Slides were then washed, dehydrated, and mounted.

Nissl staining

Slides were deparaffinised and rehydrated and after that the slides were stained in 0.5% cresyl violet solution diluted with dH_2O (ratio 1:4) until it darkens. Slides were then washed with dH_2O and differentiated in 70% ethyl alcohol with 2-3 drops of 10% acetic acid. After differentiation slides were dehydrated in 70% ethyl alcohol, followed by 96% and 100% ethyl alcohol and cleared in xylene and mounted with permanent mounting medium.

Electron microscopy
The animals were anesthetized and transcardially perfused using 6% glutaraldehyde in 0.1 M phosphate buffer. The isolated tissue samples of hippocampus and neocortex (1 STZ-icv animal treated with 3 mg/kg dose and 1 age-matched control group) were further fixed by immersion for 24 h. After postfixation in 1% OsO_4 and dehydration, the tissue was embedded in Durcupan from Fluka-Sigma Aldrich (St. Louis, MO, USA). Semithin (1 μm) and ultrathin sections (70 nm) were cut on a PowerTome XL Ultramicrotome (RMC Products). Semithin sections were stained with toluidine blue and examined by light microcopy. Ultrathin sections were contrasted with 2% uranyl acetate and with Reynolds lead citrate solution and examined by transmission electron microscope TEM 902A (Zeiss).

Ethics
Animal procedures, carried out at the University of Zagreb Medical School (Zagreb, Croatia), were in compliance with current institutional, national (The Animal Protection Act, NN135/2006; NN 47/2011), and international (Directive 2010/63/EU) guidelines governing the use of experimental animals. The experiments were approved by the national regulatory body responsible for issuing ethical approval, Croatian Ministry of Agriculture (licence No. UP/I-322-01/11-01/100 to MSP for the research approved by Croatian Ministry of Science, Education and Sport, project 108-1080003-0020), and Ethical Committee, Medical School of Zagreb (licence 380-59/11-500-77/26).

Statistics
The significance of between-group differences in the passive avoidance test (mean ± SD) was tested by Kruskall-Wallis one-way analysis of variance (ANOVA) followed by Mann-Whitney U-test, with significance set at $\alpha = 0.05$. Quantitative analysis of the signal captured by Bielschowsky silver and Nissl staining (N = 4 per group, 2 sections per brain) was done by cellSense Dimension software and further statistical analysis (mean ± SD) was done by Kruskal-Wallis and Mann-Whitney U test ($p < 0.05$).

Results

Cognitive deficits

Compared to the age-matched controls, STZ-icv rats demonstrated severe cognitive deficits manifested as lower post-shock latency time in the passive avoidance test observed from 1 to 9 months (Fig. 1). Lower latency time in STZ-icv rats indicated diminished capacity to remember that entering into the dark compartment would result in being subjected to an electric shock. Memory impairment in STZ-icv rats was clearly dose-dependent and most pronounced with the highest STZ-icv dose used (up to -95% compared to controls, $p < 0.05$; Fig. 1). Additionally, cognitive deficits were time-dependent, showing a specific time pattern of changes with all 3 doses; pronounced acute cognitive decline 1 month after STZ treatment (phase I), partial or complete improvement of memory impairment at month 3 (phase II), followed by a slow chronic cognitive decline persisiting up to 9 months after the STZ-icv treatment (phase III), which was sustained and progressive at medium and high STZ doses ($p < 0.05$; Fig. 1). Although such a time-pattern of cognitive deficits was evident with all three doses, only the lowest (0.03 mg/kg) STZ dose regime was associated with full reversibility of acute cognitive decline (latency time not different from the control group after 3 months), and partial reversibility of chronic cognitive decline (cognitive deficit persisted but was much lower in comparison to medium- and high-dose regimes, $p < 0.05$) at month 9 (Fig. 1). Analysis of individual latency time (data not shown) revealed subgroups within each STZ-icv group: subgroup 1 with latency time close to controls (298 s) and subgroup 2 with values substantially lower than controls (40-50 s). While the ratio of animals between subgroups 1 and 2 was ≤2 *vs* ≥9 in each STZ-icv treated-group at month 1, indicating a severe acute response regardless of the dose, dose-dependent reduction in subgroup 1, and increment in subgroup 2 at month 3 (7 *vs* 3, 5 *vs* 5 and 2 *vs* 8 in 0.3, 1, and 3 mg/kg group, respectively) indicated that early pathology is fully compensated in some animals but not in others of the same dose-group.

Morphological changes

Nissl and Bielschowsky silver staining showed that morphologic changes after STZ-icv treatment are dose-dependent (more pronounced with a high dose) and that the cerebral cortex is affected earlier than the corpus callosum (Figs 2, 3). Bielschowsky silver staining demonstrated fiber loss in corpus callosum with high (-31%, $p < 0.05$) and medium (-10%, $p < 0.05$) STZ-icv dose 9 months after the treatment but did not reveal any silver-stained plaques or NFTs at any of the time-points regardless of the dose (Fig. 2). Nissl staining also showed dose-dependent pathological changes in the brain of STZ-icv treated rats particularly as a reduction of cortical thickness (Fig. 3). The thickness of the parietal cortex dropped in STZ-icv treated rats 1 month after treatment with medium (-5%, $p < 0.05$) and high (-11%, $p < 0.05$) doses compared to age-matched controls, and in high-dose compared to low-dose STZ-icv rats (-11%, $p < 0.05$; Fig. 3). Although mild, the effect was stable thereafter and present in medium- and high-dose compared to low-dose STZ-icv treated rats (-7% both doses, $p < 0.05$) after 6 months and in high-dose STZ-icv treated rat compared to all other groups (-11%, $p < 0.05$) after 9 months (Fig. 3).

Amyloid pathology

Staging of amyloid pathology development in the rat brain was assessed following the treatment with high STZ-icv dose (3 mg/kg) in comparison to age-matched controls. $A\beta_{1-42}$ immunoreactivity was first seen 3 months following the STZ-icv treatment in the form of intraneuronal $A\beta_{1-42}$ accumulation in the parietal cortex (Fig. 4B, C). Extracellular $A\beta_{1-42}$ immunoreactivity in the form of aggregates that resembled human primitive plaques was

found in places in the neocortex and hippocampus 6 months following the STZ-icv treatment (Fig. 4E, H). These $A\beta_{1-42}$-positive plaque-like formations were found in higher number and concentrated in the external capsule 9 months following STZ-icv treatment (Fig. 4F, I and J). No plaque-like $A\beta_{1-42}$ immunoreactivity has been found in the control animals at any of the time-points while intraneuronal $A\beta_{1-42}$ immunoreactivity of low intensity was seen in only few cortical neurons of control rats only 9 months after icv treatment (data not shown) probably indicating some age-related $A\beta_{1-42}$ accumulation.

AT8 immunohistochemistry

Staging of tau protein pathology development in the rat brain was explored following the treatment with high STZ-icv dose (3 mg/kg) in comparison to the age-matched controls. Immunocytochemistry revealed positive AT8 signal in STZ-icv treated rats which indicated numerous early neurofibrillary changes (Fig. 5). Intracellular AT8 immunoreactivity was detected starting from 1 month after STZ-icv injection in the dispersed area of temporal cortex (Fig. 5B and C, Table 1). Interestingly, at the same time-point and at the same cortical location, much less intensive and more focused positive AT8 signal was also observed in the control animals (Fig. 5A, Table 1), Positive AT8 signal of same intensity and only at this location has been observed also in the controls at 3- and 6-month time-points and has vanished at 9-month time-point Table 1), suggesting it might be a non-specific response to icv injection. In contrast to the controls, the intensity of AT8 immunoreactivity in the temporal cortex of STZ-icv treated animals progressed with duration of the post-treatment time, and eventually started to appear additionally in the parietal cortex (Fig. E and F) and hippocampal areas CA1 and CA3 and dentate gyrus (granullar cells) where it was detected from 3 months after the STZ-icv treatment onward (Table 1). The signal was particularly intensive at 6 and 9 month-time points post STZ-icv treatment (3 mg/kg) (Fig. 5H - J, L - N). Human AD brain tissue samples were used as a positive control (data not shown).

Electron microscopy

The granule cell layer of the dentate gyrus and the external granular and pyramidal neocortical layers were assessed for ultrastructural changes by electron microscopy. The ultrastructural analysis of the selected areas showed time-dependent increase in number, size, and electron density of lysosomes in the cytoplasm of neurons from the STZ-icv (3 mg/kg) treated rat brains (Table 1), while very rare lysosomes of constant size and density were found in age-matched control animals (Fig. 6I, Table 1). In the STZ-icv treated animals the most abundant and largest lysosomes with compact dark granular content were found in the granule cell layer of the dentate gyrus 6 and 9 months after the STZ-icv treatment (Fig. 6B – D, Table 1). Unlike the cognitive and structural changes mentioned above, some ultrastructural changes were seen as early as 1 week after STZ-icv treatment (Table 1). Irregular shape of neuronal nuclei with nuclear envelope invagination as well as the presence of concentrated nucleus and nucleolus with higher electron density (pyknotic nuclei) was found starting already from 1 week after the STZ-icv treatment (Table 1). The changes progressed and were prononunced 6 and 9 months following the STZ-icv treatment (3 mg/kg) (Fig. 6F - E, Table 1). Finally, enlargement of the Golgi apparatus was observed and pronounced particularly 6 and 9 months after the STZ-icv treatment (3 mg/kg) (Fig. 6G, Table 1).

DISCUSSION

The STZ-icv rat model recapitulates most of sAD pathological features. Central administration of low STZ doses causes an insulin-resistant brain state (Agrawal et al. 2010, 2011; Chen et al. 2013; Grünblatt et al. 2007; Lester-Coll et al. 2006; Salkovic-Petrisic et al. 2006; Steen et al. 2005) which has been found also post-mortem in the brain of patients with sAD (de la Monte and Wands 2005; Frölich et al. 1999; Steen et al. 2005). Additionally, STZ-icv treated rats demonstrate cognitive deficits, glucose hypometabolism and cholinergic deficit as well as oxidative stress and astrogliosis in the brain, respectively (as reviewed elsewhere, Salkovic-Petrisic and Hoyer 2007). Beside rats, mice (Pinton et al. 2011; Plaschke et al. 2010) and monkeys (Heo et al. 2011; Park et al. 2013) also generate reproducibly these AD-like features following the STZ-icv treatment. The STZ-icv treated rat represents an inducible model that circumvents generating genetically modified animals. The follow-up of AD-like pathology onset, development, and progression in this model could contribute to elucidation of sAD ethiopathogenesis as its earliest stages remain unknown in human. So far the STZ-icv model had been characterized up to 3 months after STZ-icv administration, which is insufficient to reproduce the human disease process that takes several decades to develop. Here we present evidence of diffuse $A\beta_{1-42}$ plaque-like formations, accumulation of hyperphosphorylated AT8 tau protein and ultrastructural changes, as well as cognitive deficits, which all develop in a time- and STZ-icv dose-dependent manner during a course of 9 months.

Cognitive deficits have demonstrated a clear time pattern with acute decline observed after 1 month and a slow but progressive chronic decline seen from 3 months after STZ-icv treatment. It can be speculated that the intensive acute response seen after 1 month may reflect toxic effects of STZ (a cytotoxic compound known to induce nitrosative stress within the cell; Szkudelski 2001), which can be partly compensated until 3 months after the STZ-icv treatment (Figs 1 and 7). This tendency for compensation of acute memory impairment at 3 months demonstrated a clear dose-dependent effect. Our results indicate that a time of 3 months after the STZ-icv treatment seems to be a critical point at which the pathological processes initiated by icv injection of moderate to high STZ doses could not be compensated any longer, resulting in a slow and progressive memory decline. Additionally, measurement of cognitive deficit at 1- and 3-months demonstrated subgrouping within each STZ-icv group clearly indicating that cognitive pathology is completely compensated in a dose-dependent manner in some animals, which allows for a comparison of these early stages in STZ-icv model to mild cognitive impairment (MCI) in humans in which roughly 35% of affected patients progress to AD (Mitchell 2009). Our results are in line with the previous findings showing the individual susceptibility to streptozotocin as a characteristic feature of streptozotocin treatment in rats (Blokland and Jolles 1993; Prickaerts et al. 2000). Decompensation manifested as a late progression of cognitive decline in this model may appear as a consequence of a self-propagating destructive process in the brain which, due to a selective toxicity of STZ to insulin-producing and IR-expressing cells (Giorgino et al. 1992; Kadowaki et al. 1984; Szkudelski 2001) develops chronic insulin-resistant state with decreased glucose and energy metabolism (Salkovic-Petrisic et al. 2009). This may further lead to a dysfunction of the particular neuronal cells with dysregulation of insulin receptor signaling pathways which results in pathological accumulation of hyperphosphorylated tau protein and $A\beta_{1-42}$ and is manifested as memory decline. It seems most likely that this late, slowly developing, progressive memory decline is the one which better mimics the situation in sAD. Detection of 3 to 6-month period as a critical point after the STZ treatment has been seen in our previous research on this model also at the level of insulin degrading enzyme and glycogen synthase kinase-3β protein expression in the brain (Osmanovic-Barilar et al. 2014).

It is thus not surprising that the first morphological signs of amyloid pathology in our experiments appeared 3 months after the treatment with 3 mg/kg STZ-icv dose as intraneuronal $A\beta_{1-42}$ accumulation (Fig. 7). Our results show that it takes 6 months after the STZ-icv injection for the development of extracellular diffuse plaque-like $A\beta_{1-42}$ aggregates in rat brain (Fig. 7). Six months is also the approximate time needed for development of plaques in single-gene transgenic mice AD models that exhibit amyloid plaque pathology (*PDAPP, APP23*; McGowan et al. 2006). Six months represent approximatively 25% of a rat lifespan which, translated to humans, corresponds approximately to the development of clinical AD symptoms. To the best of our knowledge, this is the first morphological evidence of generation of diffuse plaque-like accumulation of $A\beta_{1-42}$ in the brain of non-transgenic rodents. Positive (non-aggregated) $A\beta_{1-42}$ signal in other studies was detected before 3 months but after the treatment with STZ-icv doses 13x higher (40 mg/kg; Shingo et al. 2012, 2013), which makes comparison with our data difficult.

Considering the fact that STZ induces nitroso-oxidative stress, the hypothesis that, by acting as a reactive oxygen scavenger, increased Aβ response actually limits the oxidative damage (Smith et al. 2002), fits well to the recent finding of increased $A\beta_{1-42}$ ELISA immunoreactivity detected in homogenates of rat hippocampus 5 weeks after STZ-icv administration which has caused severe mitochondrial abnormalities in the brain (Correia et al. 2013). Looking from this perspective, our results are complementary to the previously published data (Correia et al. 2013, Shingo et al. 2012). Namely, intracellular $A\beta_{1-42}$ accumulation in the rat brain as early as few weeks after the STZ-icv administration might be generated as the acute compensatory effect whose detection could be related to its intensity (depending on a STZ-icv dose), the method and $A\beta_{1-42}$ antibody used. Our experiments have shown that it takes much longer time after the STZ-icv administration for a development of a specific AD-like extracellular $A\beta_{1-42}$ accumulation. The time-course of onset and progression of CAA followed up to 9 months after the STZ-icv administration supports this finding (Salkovic-Petrisic et al. 2011). While the staging of AD by Braak and Braak (1997) is based on neuropathological criteria only, more recent additional studies suggest cerebral vascular lesions (Jellinger 2013) and CAA (Thal et al. 2002a) as of importance in the pathology of AD. While small vascular lesions do not seem to influence rates of cognitive decline in AD (Lee et al. 2000), clinicopathological studies by Grober and coworkers (Grober et al. 1999) led to the conclusion that both memory and mental status performance correlate with a modified Braak staging procedure.

Intracellular Aβ may be a product of either an intracellular synthesis, internalization from an extracellular site or perhaps a combination of both (Nixon 2007). Ineffective cellular degradation mechanisms may culminate in the progressive accumulation of aberrant protein aggregates and lysosomal burden in the AD brain (Cole et al. 1989; Haass et al. 2012). Alterations of the neuronal endosomal-lysosomal system in AD have been found to precede degenerative changes, appearing at the earliest stage as lysosomal accumulation and at more advanced AD stages as lysosomal filling with abnormally large aggregates (Cataldo et al. 1994; Pimplikar et al. 2010). In line with these data on human sAD lysosomal pathology, the ultrastructural changes presented here indicate increment in number, size, and density of lysosomes in the hippocampus and neocortex of STZ-icv treated rats. Observed ultrastructural changes correlate with and may be speculate to reflect gradual accumulation of positive $A\beta_{1-42}$ immunoreactivity in STZ-icv rats starting first intracellularly and then spreading extracellularly. This agrees with the recent evidence that Aβ may actually begin to accumulate intracellularly in lysosomes (Agholme et al. 2012; Tam and Pasternak 2012). In addition to increased lysosome numbers (Lopez et al. 2004), research in transgenic AD mice models also indicated that intracellular accumulation of $A\beta_{1-42}$ in the endosomal/lysosomal system appears either before or accompanying cognitive impairment, but well before the appearance of amyloid plaques (Knobloch et al. 2007; Wirths et al. 2001).

Hyperphosphorylation of tau protein is one of the most important AD hallmarks. We have detected increased AT8 immunoreactivity (tau protein phosphorylated at Ser202/Thr205 sites) in the parietal and temporal cortical regions as well as throughout the

hippocampus of STZ-icv treated (3 mg/kg) rats in the form of early neurofibrillary changes. As for $A\beta_{1-42}$, AT8 immunoreactivity increased in a time-dependent manner, appearing first in neocortical regions 1 month after STZ-icv treatment and spreading to the hippocampal areas (Table 1). To the best of our knowledge, this is the first *in situ* evidence of increased AT8 accumulation in STZ-icv rat model of sAD. Immunoblotting analysis has shown that 15 days after the STZ-icv treatment the expression of phospho (Ser199/202) tau protein is increased in rat neocortex and basal ganglia while no changes can be observed in the hippocampal region (Santos et al. 2012). Clinical studies indicate that tau protein is modified at the site recognized by antibody AT8 much earlier than the appearance of aggregated (fibrillar) tau, suggesting that phosphorylation at the AT8 site represents an earlier change than tau aggregation (pretangle stage) (Braak et al. 1994; Delacourte et al. 1999). These findings correlate well with our results of increased AT8 immunoreactivity but a lack of neurofibrillary tangles. Correlation of tau phosphorylation (recognized by AT8 antibody) in regions like CA3 with regression of synaptic components and memory deficits in AD patients (Spruston 2008), supports our findings of cognitive deficits in parallel with AT8 immunoreactivity from 1 month post STZ-icv treatment. Indeed improved staging procedures based on neurofibrillary pathology (Alafuzoff et al. 2008; Braak et al. 2006) correlates well with the severity of cognitive impairment (Nelson et al. 2012). Accumulation of neuropathology (tangle counts in all human brain regions) appears to correlate with global cognitive decline as patients progress from MCI to AD (Sabbagh et al. 2010). This is underlined by experimental studies in a transgenic mice AD model showing that Aβ accelerates the spatiotemporal progression of tau pathology with augmentation of tau amyloidosis (Hurtado et al. 2010).

In summary, the results presented here provide compelling evidence of the post-treatment time- and dose-dependent development of cognitive deficits, structural and ultrastructural changes, as well as diffuse $A\beta_{1-42}$ plaque-like formations and early hyperphosphorylated tau protein-related neurofibrillary changes in the STZ-icv rat model 9 months after treatment. This study provides a comprehensive staging scheme of cognitive decline and neuropathogenesis in a non-transgenic rat model generated by induction of an insulin-resistant brain state, which eventually leads to development of AD-like neuropathological changes. In line with the growing body of evidence suggesting that there may be different endophenotypes of sporadic AD (e.g. APOE4-negative individuals or pro-inflammatory phenotype /Borroni et al. 2006/), STZ-icv model might be considered as sAD endophenotype associated with insulin-resistant brain state. While respecting all limitations that animal models designed to mimic a human disease carry with them, it cannot be ignored that alterations found in STZ-icv rat model at multiple levels (cognitive, neurochemical, structural and ultrastructural) correlate well with one another and converge to model the sAD condition. Validation of STZ-icv model as a representative sAD model by taking into account the presenting staging scheme may contribute to more successful data translation from non-clinical research based on this model to clinical AD trials.

Acknowledgement

The paper is dedicated to Professor Sigfried Hoyer, the pioneer in the field of streptozotocin-induced rat model of sporadic Alzheimer's disease who greatly contributed to initiation of this research. The research was supported by the Unity Through Knowledge Fund (original UKF project 10/64), the Deutscher Akademischer Austausch Dienst (DAAD 2006-2010), the Croatian Ministry of Science, Education and Sports (grant. no. 108-1081870-1942) and the Croatian Science Foundation (grant. no. 09/16). Dr. R. Kuljis is thanked as a co-PI in the initial part of the UKF project. Prof. S. Gajovic provided help and support with electron microscopy. Dr. C. Monoranu provided helpful immunohistochemistry expertise.

The authors declare no conflict of interest.

REFERENCES

Agholme L, Hallbeck M, Benedikz E, Marcusson J, Kågedal K (2012) Amyloid-β secretion, generation, and lysosomal sequestration in response to proteasome inhibition: involvement of autophagy. J Alzheimers Dis 31:343-358.

Agrawal R, Mishra B, Tyagi E, Nath C, Shukla R (2010) Effect of curcumin on brain insulin receptors and memory functions in STZ (ICV) induced dementia model of rat. Pharmacol Res 61:247-252.

Agrawal R, Tyagi E, Shukla R, Nath C (2011) Insulin receptor signaling in rat hippocampus: a study in STZ (ICV) induced memory deficit model. Eur Neuropsychopharmacol 21:261-273.

Alafuzoff I, Arzberger T, Al-Sarraj S, Bodi I, Bogdanovic N, Braak H, Bugiani O, Del-Tredici K, Ferrer I, Gelpi E, Giaccone G, Graeber MB, Ince P, Kamphorst W, King A, Korkolopoulou P, Kovács GG, Larionov S, Meyronet D, Monoranu C, Parchi P, Patsouris E, Roggendorf W, Seilhean D, Tagliavini F, Stadelmann C, Streichenberger N, Thal DR, Wharton SB, Kretzschmar H (2008) Staging of neurofibrillary pathology in Alzheimer's disease: a study of the BrainNet Europe Consortium. Brain Pathol 18:484-496.

Bales KR (2012) The value and limitations of transgenic mouse models used in drug discovery for Alzheimer's disease: an update. Expert Opin Drug Discov 7:281-297.

Blokland A, Jolles J (1993) Spatial learni ng deficit and reduced hippocampal ChAT activity in rats after an ICV injection of streptozotocin. Pharmacol Biochem Behav 44:491-494.

Blondel O, Portha B (1989) Early appearance of in vivo insulin resistance in adult streptozotocin-injected rats. Diabete Metab 15:382-387.

Borroni B, Grassi M, Costanzi C, Archetti S, Caimi L, Padovani A (2006) APOE genotype and cholesterol levels in lewy body dementia and Alzheimer disease: investigating genotype-phenotype effect on disease risk. Am J Geriatr Psychiatry 14:1022-1031.

Braak E, Braak H, Mandelkow EM (1994) A sequence of cytoskeleton changes related to the formation of neurofibrillary tangles and neuropil threads. Acta Neuropathol 87:554-567.

Braak H, Alafuzoff I, Arzberger T, Kretzschmar H, Del Tredici K (2006) Staging of Alzheimer disease-associated neurofibrillary pathology using paraffin sections and immunocytochemistry. Acta Neuropathol 112:389-404.

Braak H, Braak E (1997) Diagnostic criteria for neuropathologic assessment of Alzheimer's disease. Neurobiol Aging 18(4 Suppl):S85-88.

Braak H, Braak E (1991) Neuropathological stageing of Alzheimer-related changes. Acta Neuropathol 82:239-259.

Braak H, Braak E (1995) Staging of Alzheimer's disease-related neurofibrillary changes. Neurobiol Aging 16:271-278.

Buee L, Bussire T, Bue-Scherrer V, Delacourte A, Hof PR (2000) Tau protein isoforms, phosphorylation and role in neurodegenerative disorders. Brain Res Rev 33:95-130.

Cataldo AM, Hamilton DJ, Nixon RA (1994) Lysosomal abnormalities in degenerating neurons link neuronal compromise to senile plaque development in Alzheimer disease. Brain Res 640:68-80.

Chen Y, Liang Z, Blanchard J, Dai CL, Sun S, Lee MH, Grundke-Iqbal I, Iqbal K, Liu F, Gong CX (2013) A non-transgenic mouse model (icv-STZ mouse) of Alzheimer's disease: similarities to and differences from the transgenic model (3xTg-AD mouse). Mol Neurobiol 47:711-725.

Cole GM, Huynh TV, Saitoh T (1989) Evidence for lysosomal processing of amyloid β-protein precursor in cultured cells. Neurochemical Research 14:933-939.

Correia SC, Santos RX, Perry G, Zhu X, Moreira PI, Smith MA (2011) Insulin-resistant brain state: The culprit in sporadic Alzheimer's disease? Ageing Res Rev 10:264-273.

Correia SC, Santos RX, Santos MS, Casadesus G, Lamanna JC, Perry G, Smith MA, Moreira PI (2013)Mitochondrial abnormalities in a streptozotocin-induced rat model of sporadic Alzheimer's disease. Curr Alzheimer Res 10:406-419.

De Felice FG, Lourenco MV, Ferreira ST (2014) How does brain insulin resistance develop in Alzheimer's disease? Alzheimers Dement 10(1 Suppl):S26-32.

de la Monte SM, Tong M (2014) Brain metabolic dysfunction at the core of Alzheimer's disease. Biochem Pharmacol 88:548-559.

de la Monte SM, Wands JR (2005) Review of insulin and insulin-like growth factor expression, signaling, and malfunction in the central nervous system: relevance to Alzheimer's disease. J Alzheimer's Dis 7:45-61.

Delacourte A, David JP, Sergeant N, Buée L, Wattez A, Vermersch P, Ghozali F, Fallet-Bianco C, Pasquier F, Lebert F, Petit H, Di Menza C (1999) The biochemical pathway of neurofibrillary degeneration in aging and Alzheimer's disease. Neurology 52:1158-1165.

Deng Y, Li B, Liu Y, Iqbal K, Grundke-Iqbal I, Gong CX (2009) Dysregulation of insulin signaling, glucose transporters, O-GlcNAcylation, and phosphorylation of tau and neurofilaments in the brain: Implication for Alzheimer's disease. Am J Pathol 175:2089-2098.

Diana A, Simic G, Sinforiani E, Orrù N, Pichiri G, Bono G (2008) Mitochondria morphology and DNA content upon sublethal exposure to beta-amyloid1-42 peptide. Coll Antropol 32 (Suppl. 1):51-58.

Frölich L, Blum-Degen D, Riederer P, Hoyer S (1999) A disturbance in the neuronal insulin receptor signal transduction in sporadic Alzheimer's disease. Ann N Y Acad Sci 893:290-293.

Giorgino F, Chen JH, Smith RJ (1992) Changes in tyrosine phosphorylation of insulin receptors and a 170,000 molecular weight nonreceptor protein in vivo in skeletal muscle of streptozotocin-induced diabetic rats: effects of insulin and glucose. Endocrinology 130:1433-1444.

Grieb P, Kryczka T, Fiedorowicz M, Frontczak-Baniewicz M, Walski M (2004) Expansion of the Golgi apparatus in rat cerebral cortex following intracerebroventricular injections of streptozotocin. Acta Neurobiol Exp (Wars) 64:481-489.

Grober E, Dickson D, Sliwinski MJ, Buschke H, Katz M, Crystal H, Lipton RB (1999) Memory and mental status correlates of modified Braak staging. Neurobiol Aging 20:573-579.

Grünblatt E, Salkovic-Petrisic M, Osmanovic J, Riederer P, Hoyer S (2007) Brain insulin system dysfunction in streptozotocin intracerebroventricularly treated rats generates hyperphosphorylated tau protein. J Neurochem 101:757-770.

Haass C, Kaether C, Thinakaran G, Sisodia S (2012) Trafficking and proteolytic processing of APP. Cold Spring Harb Perspect Med 2:a006270. doi: 10.1101/cshperspect.a006270.

Hellweg R, Nitsch R, Hock C, Jaksch M, Hoyer S (1992) Nerve growth factor and choline acetyltransferase activity levels in the rat brain following experimental impairment of cerebral glucose and energy metabolism. J Neurosci Res 31:479-486.

Heo JH, Lee SR, Lee ST, Lee KM, Oh JH, Jang DP, Chang KT, Cho ZH (2011) Spatial distribution of glucose hypometabolism induced by intracerebroventricular streptozotocin in monkeys. J Alzheimers Dis 25:517-523.

Hinrichs MH, Jalal A, Brenner B, Mandelkow E, Kumar S, Scholz T (2012) Tau protein diffuses along the microtubule lattice. J Biol Chem 287:38559-38568.

Hoyer S, Lannert H (2007) Long-term abnormalities in brain glucose/energy metabolism after inhibition of the neuronal insulin receptor: implication of tau-protein. J Neural Transm Suppl 72:195-202.

Hoyer S (2004) Glucose metabolism and insulin receptor signal transduction in Alzheimer disease. Eur J Pharmacol 490:115-125.

Hurtado DE, Molina-Porcel L, Iba M, Aboagye AK, Paul SM, Trojanowski JQ, Lee VM (2010) Aβ accelerates the spatiotemporal progression of tau pathology and augments tau amyloidosis in an Alzheimer mouse model. Am J Pathol 177:1977-1988.

Javed H, Khan MM, Khan A, Vaibhav K, Ahmad A, Khuwaja G, Ahmed ME, Raza SS, Ashafaq M, Tabassum R, Siddiqui MS, El-Agnaf OM, Safhi MM, Islam F (2011) S-allyl cysteine attenuates oxidative stress associated cognitive impairment and neurodegeneration in mouse model of streptozotocin-induced experimental dementia of Alzheimer's type. Brain Res 1389:133-142.

Jellinger KA (2013) Pathology and pathogenesis of vascular cognitive impairment-a critical update. Front Aging Neurosci 5:17. doi: 10.3389/fnagi.2013.00017

Kadowaki T, Kasuga M, Akanuma Y, Ezaki O, Takaku F (1984) Decreased autophosphorylation of the insulin receptor-kinase in streptozotocin-diabetic rats. J Biol Chem 259:14208-14216.

Knobloch M, Konietzko U, Krebs DC, Nitsch RM (2007) Intracellular Abeta and cognitive deficits precede beta-amyloid deposition in transgenic arcAbeta mice. Neurobiol Aging 28:1297-1306.

Kosaraju J, Gali CC, Khatwal RB, Dubala A, Chinni S, Holsinger RM, Madhunapantula VS, Muthureddy Nataraj SK, Basavan D (2013) Saxagliptin: A dipeptidyl peptidase-4 inhibitor ameliorates streptozotocin induced Alzheimer's disease. Neuropharmacology 72:291-300.

Kraska A, Santin MD, Dorieux O, Joseph-Mathurin N, Bourrin E, Petit F, Jan C, Chaigneau M, Hantraye P, Lestage P, Dhenain M (2012) In vivo cross-sectional characterization of cerebral alterations induced by intracerebroventricular administration of streptozotocin. PLoS One 7:e46196. doi: 10.1371/journal.pone.0046196.

Lackovic Z, Salkovic M (1990) Streptozotocin and alloxan produce alterations in rat brain monoamines independently of pancreatic beta cells destruction. Life Sci 46:49-54.

Lannert H, Hoyer S (1998) Intracerebroventricular administration of streptozotocin causes long-term diminutions in learning and memory abilities and in cerebral energy metabolism in adult rats. Behav Neurosci 112:1199-1208.

Lee JH, Olichney JM, Hansen LA, Hofstetter CR, Thal LJ (2000) Small concomitant vascular lesions do not influence rates of cognitive decline in patients with Alzheimer disease. Arch Neurol 57:1474-1479.

Lester-Coll N, Rivera EJ, Soscia SJ, Doiron K, Wands JR, de la Monte S (2006) Intracerebral streptozotocin model of type 3 diabetes: Relevance to sporadic Alzheimer's disease. J Alzheimer's Dis 9:13-33.

Leuner K, Müller WE, Reichert AS (2012). From mitochondrial dysfunction to amyloid beta formation: novel insights into the pathogenesis of Alzheimer's disease. Mol Neurobiol 46:186-193.

Lithner CU, Hedberg MM, Nordberg A (2011) Transgenic mice as a model for Alzheimer's disease. Curr Alzheimer Res 8:818-831.

Lopez EM, Bell KF, Ribeiro-da-Silva A, Cuello AC (2004) Early changes in neurons of the hippocampus and neocortex in transgenic rats expressing intracellular human a-beta. J Alzheimers Dis 6:421-431.

Mayer G, Nitsch R, Hoyer S (1990) Effects of changes in peripheral and cerebral glucose metabolism on locomotor activity, learning and memory in adult male rats. Brain Res 532:95-100.

McGowan E, Eriksen J, Hutton M (2006) A decade of modeling Alzheimer's disease in transgenic mice. Trends Genet 22:281-289.

Mitchell AJ (2009) CSF phosphorylated tau in the diagnosis and prognosis of mild cognitive impairment and Alzheimer's disease: a meta-analysis of 51 studies. J Neurol Neurosurg Psychiatr 80:966–975.

Nelson PT, Alafuzoff I, Bigio EH, Bouras C, Braak H, Cairns NJ, Castellani RJ, Crain BJ, Davies P, Del Tredici K, Duyckaerts C, Frosch MP, Haroutunian V, Hof PR, Hulette CM, Hyman BT, Iwatsubo T, Jellinger KA, Jicha GA, Kövari E, Kukull WA, Leverenz JB, Love S, Mackenzie IR, Mann DM, Masliah E, McKee AC, Montine TJ, Morris JC, Schneider JA, Sonnen JA, Thal DR, Trojanowski JQ, Troncoso JC, Wisniewski T, Woltjer RL, Beach TG (2012) Correlation of Alzheimer disease neuropathologic changes with cognitive status: a review of the literature. J Neuropathol Exp Neurol 71:362-381.

Nitsch R, Hoyer S (1991) Local action of the diabetogenic drug streptozotocin on glucose and energy metabolism in rat brain cortex. Neurosci Lett 128:199-202.

Niwa K, Kazama K, Younkin SG, Carlson GA, Iadecola C (2002) Alterations in cerebral blood flow and glucose utilization in mice overexpressing the amyloid precursor protein. Neurobiol Dis 9:61-68.

Nixon RA (2007) Autophagy, amyloidogenesis and Alzheimer disease. J Cell Sci 120:4081-4091.

Noble EP, Wurtman RJ, Axelrod J (1967) A simple and rapid method for injecting H3-norepinephrine into the lateral ventricle of the rat brain. Life Sci 6:281-291.

Osmanovic Barilar J, Knezovic A, Grünblatt E, Riederer P, Salkovic-Petrisic M (2014) Nine-month follow-up of the insulin receptor signalling cascade in the brain of streptozotocin

rat model of sporadic Alzheimer's disease. J Neural Transm [Epub ahead of print] DOI 10.1007/s00702-014-1323-y

Park SJ, Kim YH, Lee Y, Kim KM, Kim HS, Lee SR, Kim SU, Kim SH, Kim JS, Jeong KJ, Lee KM, Huh JW, Chang KT (2013) Selection of appropriate reference genes for RT-qPCR analysis in a streptozotocin-induced Alzheimer's disease model of cynomolgus monkeys (Macaca fascicularis). PLoS One 8:e56034. doi: 10.1371/journal.pone.0056034.

Pedersen WA, McMillan PJ, Klustad JJ, Leverenz JB, Craft S, Haynatzki GR (2006) Rosiglitazone attenuates learning and memory deficits in Tg2576 Alzheimer mice. Exp. Neurol 199:265-273.

Pedrós I, Petrov D, Allgaier M, Sureda F, Barroso E, Beas-Zarate C, Auladell C, Pallàs M, Vázquez-Carrera M, Casadesús G, Folch J, Camins A (2014) Early alterations in energy metabolism in the hippocampus of APPswe/PS1dE9 mouse model of Alzheimer's disease. Biochim Biophys Acta 1842:1556-1566.

Pimplikar SW, Nixon RA, Robakis NK, Shen J, Tsai LH (2010) Amyloid-independent mechanisms in Alzheimer's disease pathogenesis. J Neurosci 30:14946-14954.

Pinton S, da Rocha JT, Gai BM, Nogueira CW (1993) Sporadic dementia of Alzheimer's type induced by streptozotocin promotes anxiogenic behavior in mice. Behav Brain Res 223:1-6.

Plaschke K, Hoyer S (1993) Action of the diabetogenic drug streptozotocin on glycolytic and glycogenolytic metabolism in adult rat brain cortex and hippocampus. Int J Dev Neurosci 11:477-483.

Plaschke K, Kopitz J, Siegelin M, Schliebs R, Salkovic-Petrisic M, Riederer P, Hoyer S (2010) Insulin-resistant brain state after intracerebroventricular streptozotocin injection exacerbates Alzheimer-like changes in Tg2576 AbetaPP-overexpressing mice. J Alzheimers Dis 19:691-704.

Prickaerts J, De Vente J, Honig W, Steinbusch H, Ittersum MMV, Blokland A, Steinbusch HW (2000) Nitric oxide synthase does not mediate neurotoxicity after an i.c.v. injection of streptozotocin in the rat. J Neural Transm 107:745-766.

Prickaerts J, Fahrig T, Blokland A (1999) Cognitive performance and biochemical markers in septum, hippocampus and striatum of rats after an i.c.v. injection of streptozotocin: a correlation analysis. Behav Brain Res 102:73-88.

Rodrigues L, Dutra MF, Ilha J, Biasibetti R, Quincozes-Santos A, Leite MC, Marcuzzo S, Achaval M, Gonçalves CA (2010) Treadmill training restores spatial cognitive deficits and neurochemical alterations in the hippocampus of rats submitted to an intracerebroventricular administration of streptozotocin. J Neural Transm 117:1295-1305.

Sabbagh MN, Cooper K, DeLange J, Stoehr JD, Thind K, Lahti T, Reisberg B, Sue L, Vedders L, Fleming SR, Beach TG (2010) Functional, global and cognitive decline correlates to accumulation of Alzheimer's pathology in MCI and AD. Curr Alzheimer Res 7:280-286.

Salkovic M, Sabolic I, Lackovic Z (1995) Striatal dopaminergic D1 and D2 receptors after intracerebroventricular application of alloxan and streptozotocin in rat. J Neural Transm Gen Sect 100:137-145.

Salkovic-Petrisic M, Hoyer S (2007) Central insulin resistance as a trigger for sporadic Alzheimer-like pathology: an experimental approach. J Neural Transm Suppl 72:217-233.

Salkovic-Petrisic M, Knezovic A, Hoyer S, Riederer P (2013) What have we learned from the streptozotocin-induced animal model of sporadic Alzheimer's disease, about the therapeutic strategies in Alzheimer's research. J Neural Transm 120:233-252.

Salkovic-Petrisic M, Osmanovic J, Grünblatt E, Riederer P, Hoyer S (2009) Modeling Sporadic Alzheimer's Disease: The Insulin Resistant Brain State generates Multiple Long-Term Morphobiological Abnormalities Inclusive Hyperphosphorylated Tau Protein and Amyloid-β. A Synthesis. J Alzheimer's Dis 18:729-750.

Salkovic-Petrisic M, Osmanovic-Barilar J, Brückner MK, Hoyer S, Arendt T, Riederer P (2011) Cerebral amyloid angiopathy in streptozotocin rat model of sporadic Alzheimer's disease: a long-term follow up study. J Neural Transm 118:765-772.

Salkovic-Petrisic M, Tribl F, Schmidt M, Hoyer S, Riederer P (2006) Alzheimer-like changes in protein kinase B and glycogen synthase kinase-3 in rat frontal cortex and hippocampus after damage to the insulin signalling pathway. J Neurochem 96:1005-1015.

Santos TO, Mazucanti CH, Xavier GF, Torrão AS (2012) Early and late neurodegeneration and memory disruption after intracerebroventricular streptozotocin. Physiol Behav 107:401-413.

Selkoe DJ (2001) Alzheimer's disease results from the cerebral accumulation and cytotoxicity of amyloid beta-protein. J Alzheimers Dis 3:75-80.

Sharma M, Gupta YK (2001) Intracerebroventricular injection of streptozotocin in rats produces both oxidative stress in the brain and cognitive impairment. Life Sci 68:1021-1029.

Shaw CA, Höglinger GU (2008) Neurodegenerative diseases: neurotoxins as sufficient etiologic agents? Neuromolecular Med 10:1-9.

Shingo AS, Kanabayashi T, Kito S, Murase T (2013) Intracerebroventricular administration of an insulin analogue recovers STZ-induced cognitive decline in rats. Behav Brain Res 241:105-111.

Shingo AS, Kanabayashi T, Murase T, Kito S (2012) Cognitive decline in STZ-3V rats is largely due to dysfunctional insulin signalling through the dentate gyrus. Behav Brain Res 229:378-383.

Shoham S, Bejar C, Kovalev E, Schorer-Apelbaum D, Weinstock M (2007) Ladostigil prevents gliosis, oxidative-nitrative stress and memory deficits induced by intracerebroventricular injection of streptozotocin in rats. Neuropharmacology 52:836-843.

Shoham S, Bejar C, Kovalev E, Weinstock M (2003) Intracerebroventricular injection of streptozotocin causes neurotoxicity to myelin that contributes to spatial memory deficits in rats. Exp Neurol 84:1043-1052.

Simic G, Gnjidic M, Kostovic I (1998) Cytoskeletal changes as an alternative view on pathogenesis of Alzheimer's disease. Period Biol 100:165-173.

Simic G, Stanic G, Mladinov M, Jovanov-Milosevic N, Kostovic I, Hof PR (2009) Does Alzheimer's disease begin in the brainstem? Neuropathol Appl Neurobiol 35:532-554.

Smith MA, Drew KL, Nunomura A, Takeda A, Hirai K, Zhu X, Atwood CS, Raina AK, Rottkamp CA, Sayre LM, Friedland RP, Perry G (2002) Amyloid-beta, tau alterations and mitochondrial dysfunction in Alzheimer disease: the chickens or the eggs? Neurochem Int 40:527-531.

Spruston N (2008) Pyramidal neurons: dendritic structure and synaptic integration. Nat Rev Neurosci 9:206-221.

Steen E, Terry BM, Rivera EJ, Cannon JL, Neely TR, Tavares R, Xu XJ, Wands JR, de la Monte SM (2005) Impaired insulin and insulin-like growth factor expression and signaling mechanisms in Alzheimer's disease--is this type 3 diabetes? J Alzheimers Dis 7:63-80.

Szkudelski T (2001) The mechanism of alloxan and streptozotocin action in B cell of the rat pancreas. Physiol Res 50:537-546.

Tam JH, Pasternak SH (2012) Amyloid and Alzheimer's disease: inside and out. Can J Neurol Sci 39:286-298.

Thal DR, Ghebremedhin E, Rüb U, Yamaguchi H, Del Tredici K, Braak H (2002a) Two types of sporadic cerebral amyloid angiopathy. J Neuropathol Exp Neurol 61:282-293.

Thal DR, Rüb U, Orantes M, Braak H (2002b) Phases of A beta-deposition in the human brain and its relevance for the development of AD. Neurology 58:1791-1800.

Thome J, Gsell W, Rösler M, Kornhuber J, Frölich L, Hashimoto E, Zielke B, Wiesbeck GA, Riederer P (1997) Oxidative-stress associated parameters (lactoferrin, superoxide dismutases) in serum of patients with Alzheimer's disease. Life Sci 60:13-19.

Uchihara T (2007) Silver diagnosis in neuropathology: principles, practice and revised interpretation. Acta Neuropathol 13:483-499.

Völkel W, Sicilia T, Pähler A, Gsell W, Tatschner T, Jellinger K, Leblhuber F, Riederer P, Lutz WK, Götz ME (2006) Increased brain levels of 4-hydroxy-2-nonenal glutathione conjugates in severe Alzheimer's disease. Neurochem Int 48:679-686.

Wirths O, Multhaup G, Czech C, Blanchard V, Moussaoui S, Tremp G, Pradier L, Beyreuther K, Bayer TA (2001) Intraneuronal Abeta accumulation precedes plaque formation in beta-amyloid precursor protein and presenilin-1 double-transgenic mice. Neurosci Lett 306:116-120.

Zahs KR, Ashe KH (2010) 'Too much good news' - are Alzheimer mouse models trying to tell us how to prevent, not cure, Alzheimer's disease? Trends Neurosci 33:381-389.

FIGURE LEGENDS:

Table 1 Summary of semiquantitative assessment / staging of the neuropathological and ultrastructural findings in the STZ-icv rat model

TREATMENT		TIME AFTER STZ-ICV TREATMENT				
		1 week	1 month	3 months	6 months	9 months
Control (citrate buffer-icv)	Aβ1-42	0	0	0	0	0
	AT8	0	1 (TC)	1 (TC)	1 (TC)	1
	EM	0 (L), 1 (N)	0 (L), 1 (N)	0 (L), 1 (N)	0 (L), 1 (N)	0 (L), 1 (N)
STZ-icv (3 mg/kg)	Aβ1-42	0	0	0.25 (PC)	0-3 (PC, HPC)	0-3 (PC,HPC)
	AT8	0	3 (TC)	4 (TC, HPC)	4-5 (TC,PC,CA3,CA1)	4-5 (TC,PC,CA3)
	EM	1 (L, N)	1(N), 2(L)	1 (N), 3 (L)	1 (PN),2 (N), 3 (G), 4 (L)	2 (PN), 3 (N),5 (L, G)

SCALE OF CHANGES IN IMMUNOHSITOCHEMISTRY (IHC) STAINING OF AMYLOID β 1-42 (Aβ1-42) AND HYPERPHOSPHORYLATED TAU PROTEIN (AT8) AND IN ULTRASTRUCTURAL ELECTRON MICROSCOPY OF HIPPOCAMPAL AND CORTICAL NEURONES:

	Aβ1-42 immunohistochemistry	AT8 immunohistochemistry	electron microscopy
0	no staining (no histopathological changes)	no staining (no histopathological changes)	no ultrastructural changes
1	no or very weak Aβ1-42 staining in scarce neurons in hippocampal CA1 region	no or weak AT8 staining in scarce neurons in selected regions	very scarce presence of lysososmes (L), very scarce presence of neuronal nuclei irregular in shape (N), concentrated nucleus and nucleolus with higher electron density (pyknotic nuclei) (PN)
2	weak Aβ1-42 staining (amyloid deposits, denoting potential earliest changes)	weak AT8 staining in some neurons in selected regions	scarce presence of lysosomes (L), scarce presence of neuronal nuclei irregular in shape with mild nuclear envelope invagination (N), frequent presence of concentrated nucleus and nucleolus with higher electron density (pyknotic nuclei) (PN)
3	moderate Aβ1-42 staining (amyloid deposits, denoting potential earliest changes)	weak to moderate AT8 staining (in a single region, denoting early neurofibrillary changes i.e. early neurofibrillary tangles, dystrophic neurites and/or neuropil threads)	not very abundant lysosomes of medium large size and electronic density (L), presence of neuronal nuclei irregular in shape with nuclear envelope invagination (N), enlargement of the Golgi apparatus (G)
4	moderate Aβ1-42 staining in several regions	moderate AT8 staining in several regions or level 1 changes +presence of amyloid plaques	abundant, large and electronically dense lysosomes (L),
5	late changes (presence of both neurofibrillary changes and plaque-like formations in many brain regions/areas)	late changes (presence of both neurofibrillary changes and plaque-like formations in many brain regions/areas)	very abundant, large and electronically dense lysosomes (L), extensive enlargement of the Golgi apparatus (G)

TC, temporal cortex; PC, parietal cortex; HPC, hippocampus; CA1 and CA3, regions of hippocampus; EM, electron microscopy; STZ-icv, streptozotocin-itracerebroventricularly treated rats

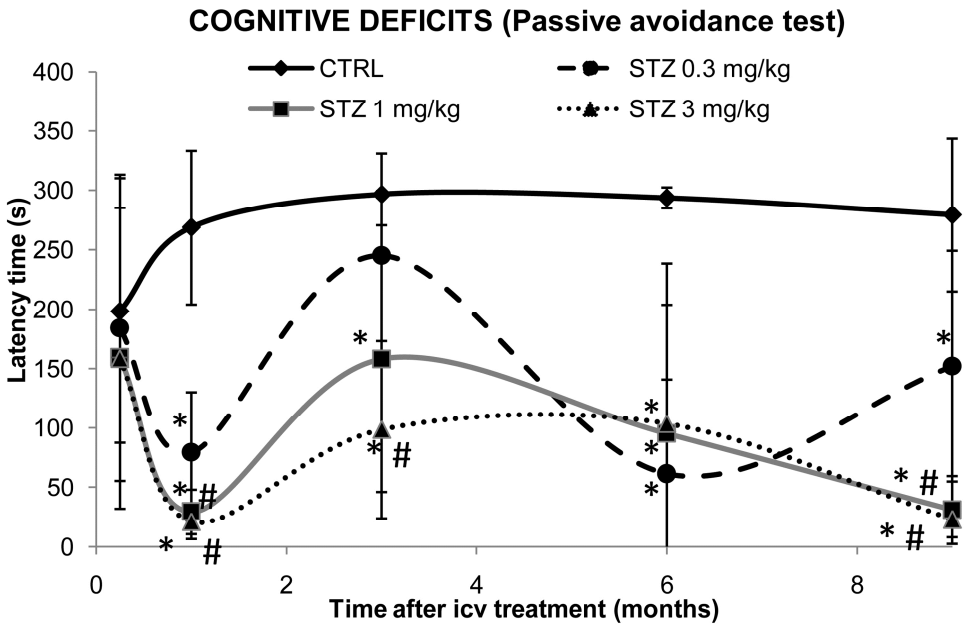

Fig. 1 Nine-month follow-up of cognitive deficits in STZ-icv rat model measured in Passive Avoidance test. Streptozotocin (STZ) -treated and age-matched control (CTRL) rats were subjected to Passive Avoidance test in which latency time (s) to entering the dark compartment was recorded on the third testing day. Cognitive deficits manifested as lower latency time in comparison to the age-matched control were determined for three STZ dose regimens (0.3, 1 and 3 mg/kg) at 5 time-points after the treatment (1 week, and 1, 3, 6, and 9 months). Each point represents mean ± SD of the particular group (N = 8-10). Data were analyzed by Kruskal-Wallis ANOVA followed by Mann-Whitney U test: *$p < 0.05$ vs respective CTRL group at each time-point; #$p < 0.05$ vs STZ 0.03 mg/kg group at each time-point

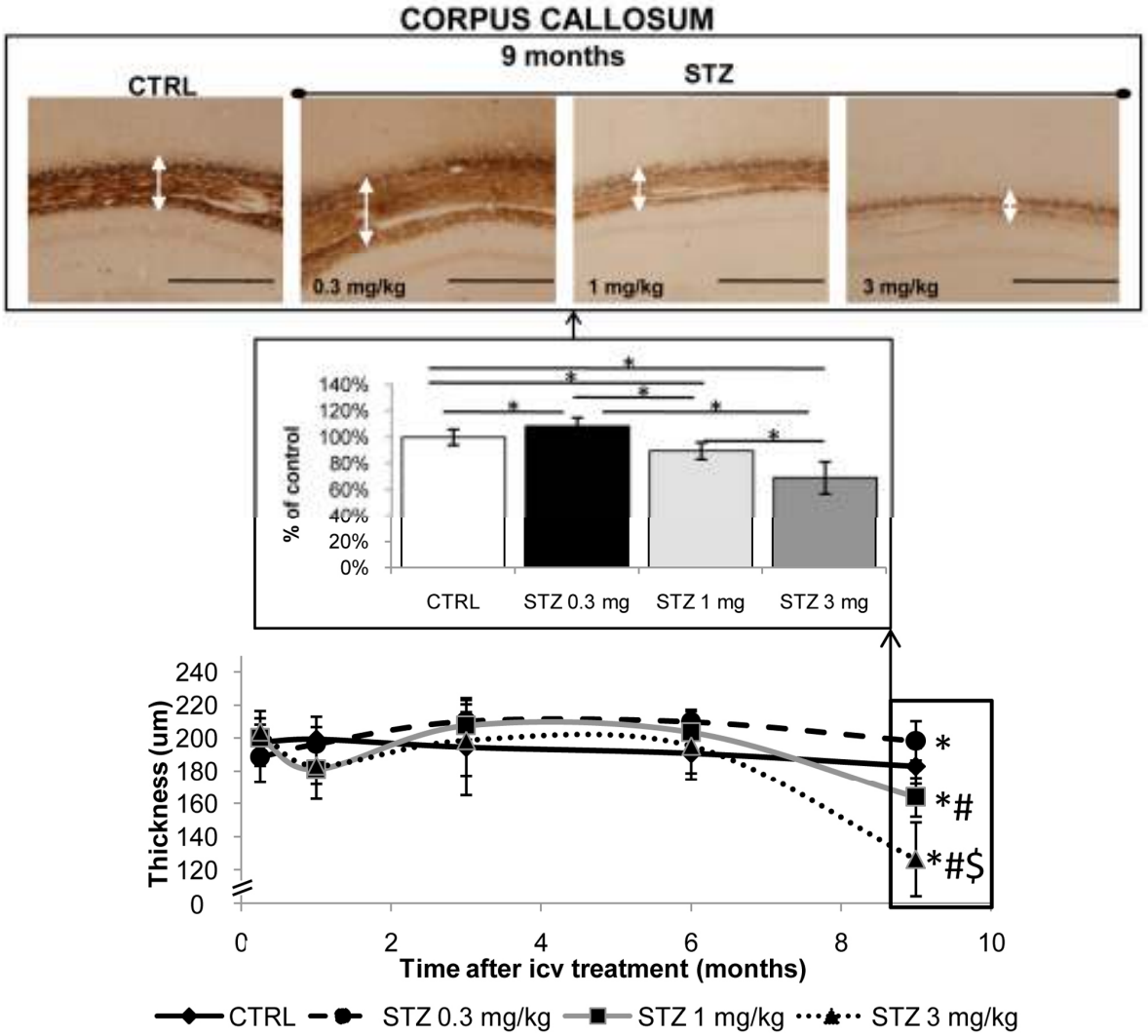

Fig. 2 Staging of fibre loss in the rat corpus callosum following streptozotocin treatment (Bielschowsky silver staining). Quantitative analysis of thickness of the corpus callosum from the streptozotocin (STZ)-treated (0.3, 1, and 3 mg/kg) and age-matched control (CTRL) rats collected 1 week, and 1, 3, 6, and 9 months following the icv treatment is presented as a time-curve with statistically significant changes presented additionally as bars (mean ± SD), *p < 0.05 by Kruskal-Wallis and Mann-Whitney U test. Since the significant difference between the groups by Kruskal-Wallis test was detected only at 9-month time point only, respective (representative) microphotographs of the brain from the STZ (0.3, 1, and 3 mg/kg) and age-matched CTRL rats collected 9 months following the icv treatment are presented only. White arrows on microphotographs point to the corpus callosum. Images were taken at matching coronal level. Scale bar = 500 μm

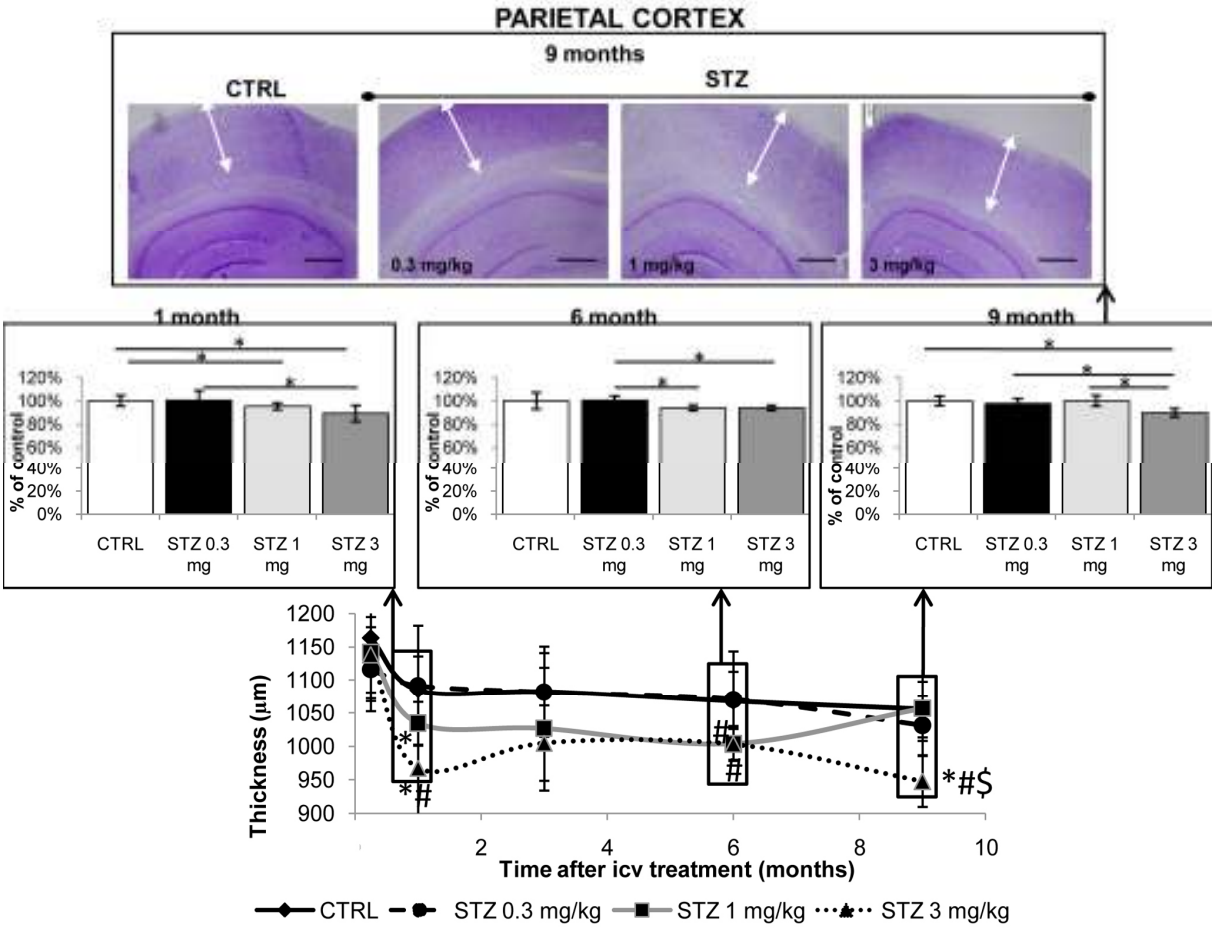

Fig. 3 Staging of the cortical loss following streptozotocin treatment in rats (Nissl staining). Quantitative analysis of thickness of the parietal cortex from the streptozotocin (STZ)-treated (0.3, 1, and 3 mg/kg) and age-matched control (CTRL) rats collected 1 week, 1 month, 3, 6 and 9 months following the icv treatment is presented as a time-curve with statistically significant changes presented additionally as bars (mean ± SD), *p < 0.05 by Kruskal-Wallis and Mann-Whitney U test. The significant difference between the groups by Kruskal Wallis test was detected at 1, 3 and 9-month time points and respective (representative) microphotographs of the brain from the STZ-icv treated (0.3, 1, and 3 mg/kg) and age-matched control rats are presented as well. Black arrows on microphotographs point to the parietal cortex. Images were taken at matching coronal level. Scale bar = 500 µm

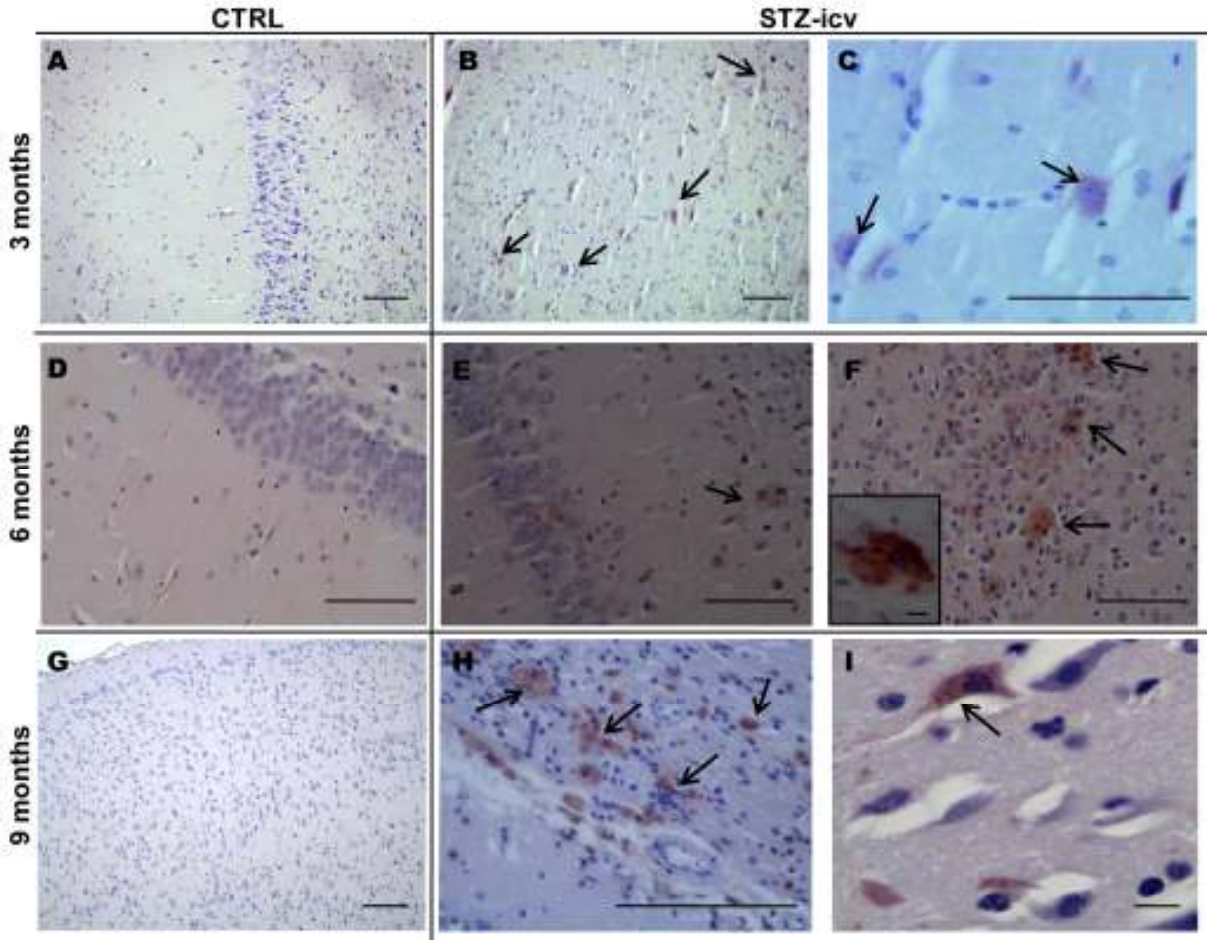

Fig. 4 $A\beta_{1-42}$ accumulation of in the brain of STZ-icv treated rats, visualized by $A\beta_{1-42}$ immunohistochemistry. The figure shows representative microphotographs of the brain from the streptozotocin (STZ, 3 mg/kg)-treated rats and age-matched controls (CTRL) **(A, D, G)** obtained 3, 6 and 9 months following the treatment, respectively. Three months following the STZ treatment positive signal revealed only intracellular $A\beta_{1-42}$ accumulation in the parietal cortex **(B, C)** while starting from the 6-month time-point **(E, F)** up to 9 months **(H, I)**, positive signals of both intra- and extracellular primitive plaque-like $A\beta_{1-42}$ accumulation were found predominantly in the parietal cortex **(F -small insert)** and to a lesser extent in the hippocampus. Scale bar = 100 μm, except for Fig. 4I and a small insert at Fig. 4F: scale bar = 10 μm

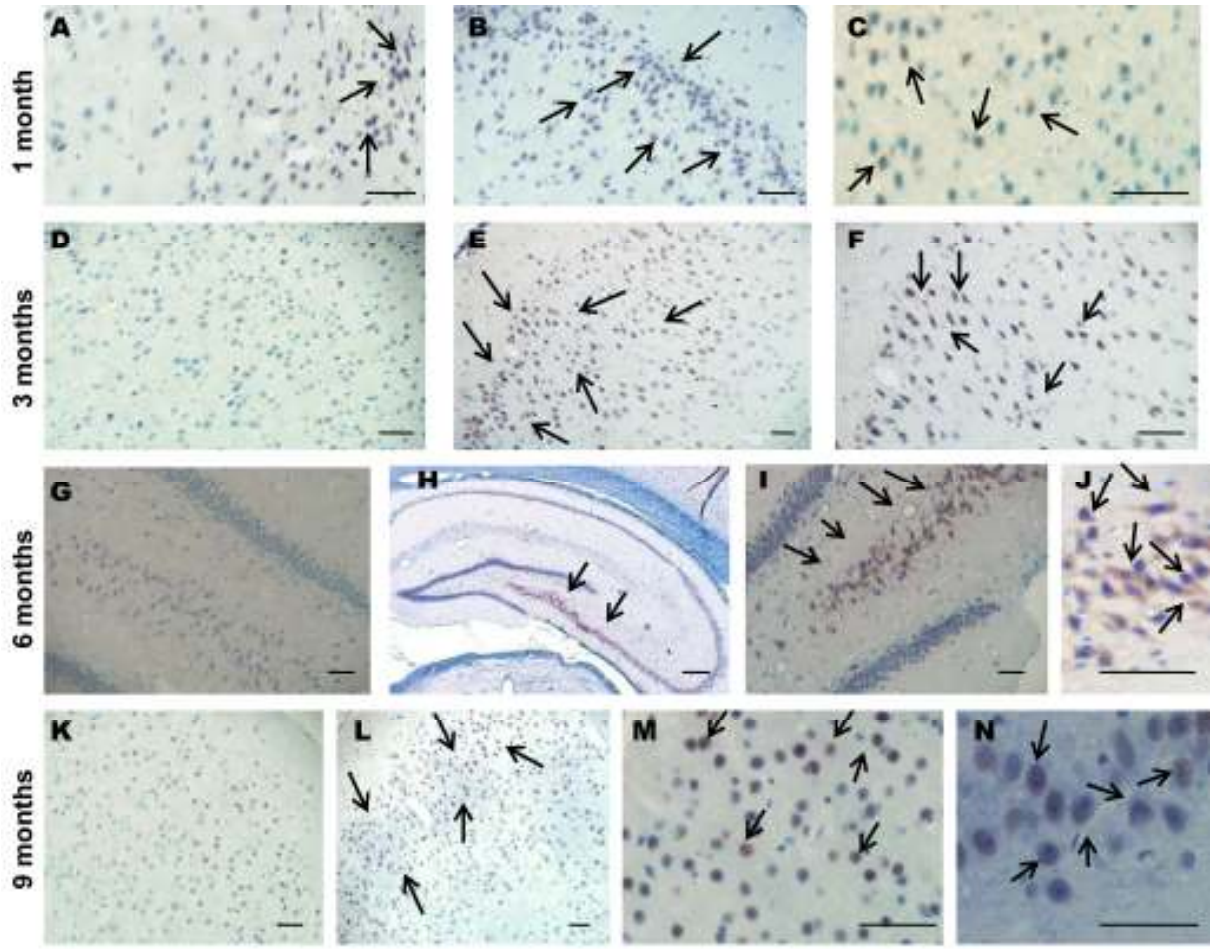

Fig. 5 Immunoreactivity of hyperphosphorylated tau protein in the brain of STZ-icv treated rats, visualized by AT8 immunohistochemistry. The figure shows representative microphotographs of the brain from the streptozotocin (STZ, 3 mg/kg)-treated rats (B, C, E, F, H – J, L – N) and age-matched controls (CTRL) **(A, D, G, K)** obtained 1 month, 3, 6 and 9 months following the treatment. Representative microphotographs present intracellular AT8 immunoreactivity seen in the hippocampal CA3 region (**H - J,** 6 months), granular cell layer of the dentate gyrus (**N**, 9 months) and in the parietal cortex (**B and C,** 1 month; **E** and F, 3 months; **L** and M, 9 months). Scale bar = 50 μm, except for Fig. 5H: scale bar = 200 μm

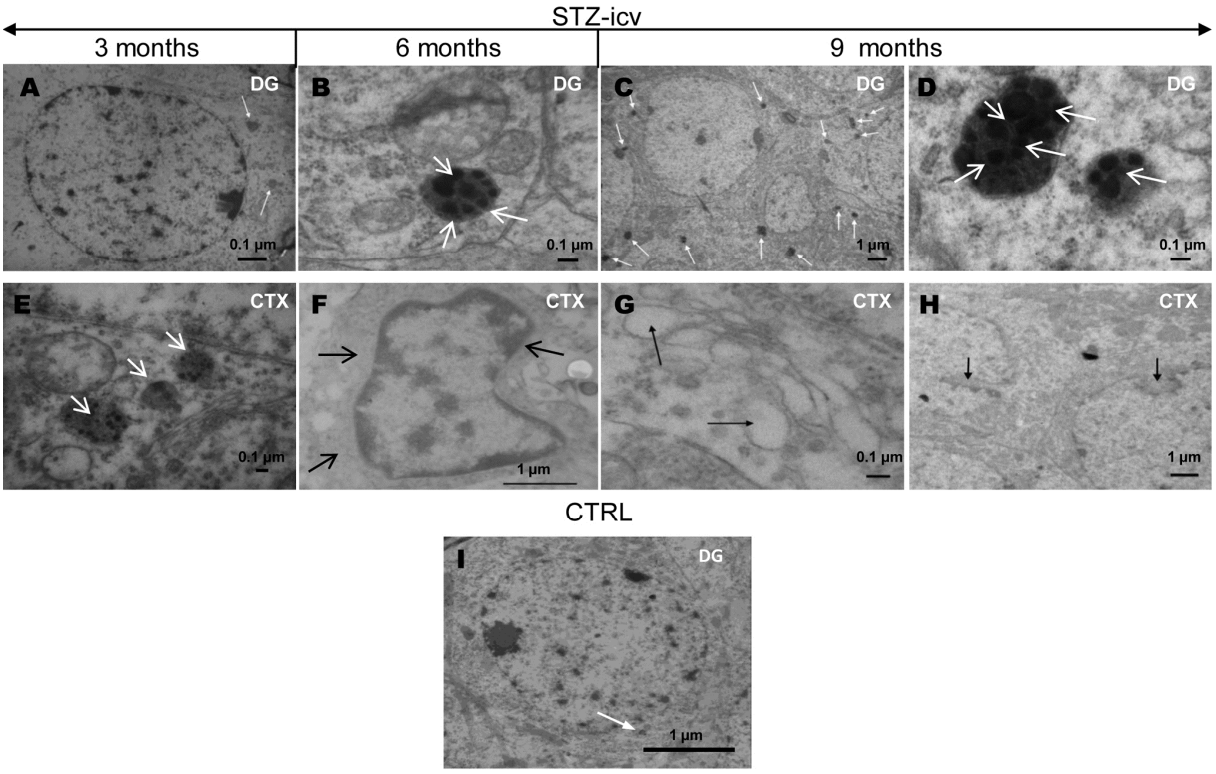

Fig. 6 Ultrastructural changes in the brain of STZ-icv treated rats. The figure shows representative microphotographs of the neurons in (**A – D**) the granule cell layer of the dentate gyrus (DG) and (**E – H**) the pyramidal layers (CTX) in the streptozotocin (STZ, 3 mg/kg)-treated rats obtained 3, 6 and 9 months following the treatment. Representative microphotograph of control (CTRL) rats (6-month time-point) is presented for comparison (**I**). The photomicrographs show the lysosomes and their dark granular content marked with white arrows (**A – E**), and pyknotic nucleus (**F**), enlargement of the Golgi apparatus with swollen terminal cisternae (**G**) and nuclear envelope invaginations (**H**) marked with black arrows. Scale bar is marked at each microphotograph

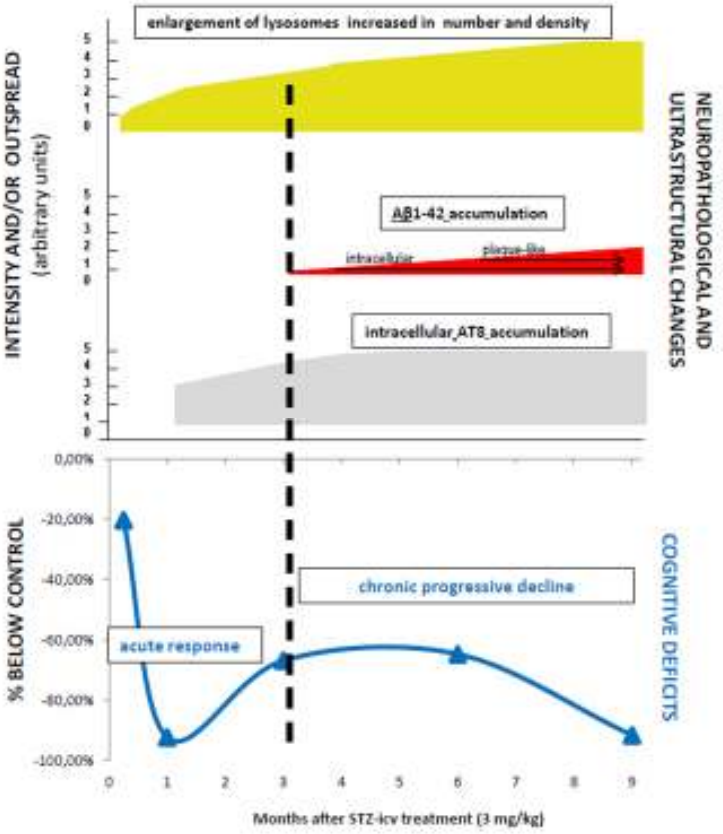

Fig. 7 Staging of cognitive deficits and underlying neuropathological and ultrastructural changes in the brain of a STZ-icv rat model. The figure presents the correlation of staging of cognitive deficits and structural/ultrastructural changes in a streptozotocin (STZ)-induced rat model of sporadic Alzheimer's disease (sAD). Data present findings obtained in animals treated intracerebroventricularly (icv) with 3 mg/kg STZ dose. Ultrastructural changes (pyknotic nuclei, lysosomal changes) of mild intensity appeared before (starting from 1 week after the STZ treatment) the structural changes and cognitive deficits in this experimental design (both starting from 1 month after the STZ treatment). The order of appearance in the 9-month post STZ-treatment period (from the earliest to the latest event) was: ultrastructural changes < early neurofybrillary changes (AT8) and acute cognitive decline < intracellular amyloid $\beta_{1\text{-}42}$ accumulation < extracellular plaque-like $A\beta_{1\text{-}42}$ accumulation and chronic progressive cognitive decline. While ultrastructural and structural changes were both slowly progressing in the course of time, the cognitive deficits followed a triphasic pattern; (I) acute decline, (II) partial amelioration of cognitive decline, (III) chronic progressive cognitive decline. Three months after the STZ treatment seemed to be a critical point at which the pathological processes initiated by high STZ dose (3 mg/kg) could not be compensated any longer, resulting in a slow and progressive memory decline which correlated well with the first appearance of pathological Aβ accumulation. Not only that pathological Aβ accumulation appeared later than tau protein-related neurofibrillary changes and ultrastructural abnormalities, based on the arbitrary unit scale (0-5), it was also of the lower intensity 9 months after the STZ treatment compared to neurofibrillary and ultrastructural changes (≤ 3 vs ≤ 5). Considering the structural and ultrastructural changes observed in this 9-month follow-up, it seems most likely that the late, slowly developing, progressive memory decline in the STZ-icv rat model is the one which better mimics the situation in sAD